(2)

Annual Report

ONR Grant No: N00014-91-J-1299

DEVELOPMENT OF THE MICROSTRUCTURE BASED STOCHASTIC LIFE PREDICTION MODELS

Prepared by : Prof. Marek A. Przystupa (Principal Investigator),
Jimin Zhang and Annetta J. Luevano
Department of Material Science and Engineering
University of California
Los Angeles, CA 90024
Tel.: (310) 825-6559
FAX: (310) 206-7353

Submitted to: Dr. A. K. Vasudevan
Program Manager, Mechanics and Materials
Applied Research & Technology
Office of Naval Research
800 North Quincy Street, Code 1216
Arlington, VA 22217-5000

February 10, 1992

ABSTRACT

The purpose of the fatigue life prediction program at UCLA is to characterize the accumulation of the microstructural damage during fatigue of the aluminum alloys and to use obtained data in the formulation of the microstructure based stochastic life prediction models. Emphasis during the first year of the program was on the implementation of all required quantitative microscopy techniques and on the characterization of the starting microstructures in the "high" and "low" porosity 7050-T7451 commercial plate alloys. The first assembled set of data includes characteristics of the grain structures, constituent particles and pores on the sections parallel to the plate surface as a function of the distance from the surface. The results show that both alloys have partially recrystallized structure with the recrystallization levels changing from zero at the surface to about 20% in the center. The unrecrystallized grains are 85 to 240 μm in size, while for the recrystallized ones the sizes are in the 45 to 85 μm range. The average pore size is 7.74 μm for the high porosity alloy and 7.15 μm for the low porosity material with the area fractions of 0.074% and 0.072% respectively. The sizes of the constituent particles are 8.38 and 8.21 μm and the area fractions 0.88% and 0.65% for the high and low porosity alloys respectively. Preliminary results from the tessellation analysis indicate that the pores have spatial distribution which can be categorized as regular with clusters. For the constituent particles the distributions are clustered. A number of the constituent particles have cracks and the measurements of their frequency are in progress. The most common precipitate phases present in the alloy are η', η_1, η_2 and η_4. The precipitates inside the grains are small ranging from 5 to 45 nm in diameters while precipitates on the grain boundaries are generally larger and their sizes vary between 20 - 250 nm. Precipitate free zones have been also observed and the measurements of their characteristics are in progress. The theoretical efforts during the first year of the program have been limited to the literature survey of the available stochastic life prediction models and to the development of a preliminary Markov chain model. Plans for the 1992 include finishing characterization of the 7050 alloys, formulation of the preliminary life prediction models and start of the characterizations of the 8090 alloys.

CONTENTS

A. Introduction

The purpose of this report is to describe the status of the fatigue life prediction program at UCLA. The program started in December 1990 and its main objectives were characterization of the accumulation of microstructural damage during fatigue of aluminum alloys and formulation of the microstructure based stochastic life prediction models based on those characterizations[1]. The emphases during the reporting period were (1) on the test and implementation of the microstructure characterization techniques and (2) on the characterization of the microstructures of the "high" and "low" porosity 7050-T7451 commercial plate alloys. We have accomplished all our goals for the 1991 and this report gives account for our activities and accomplishments and summarizes our plans the 1992.

B. Materials

As reported earlier [2] the materials investigated during the first year of the program were "high" porosity (old pedigree) and "low" porosity (new pedigree) 7050-T7451 alloys. The samples were obtained from Alcoa Laboratories as a result of the Alcoa/UCLA/ONR collaboration on the program. Up to date we have completed quantification of the grain structures, constituent particles and pores on the surface sections of the as-received plates (characterizations on other sections are in progress). We have also characterized the morphology of the precipitates in both alloys.

C. Quantitative Techniques

In order to formulate stochastic life prediction models it is not sufficient to know only the average values of the microstructural parameters, but it is also essential to know their frequancy distributions. Our approach toward that end was to put together a PC-based image analysis system and develop a set of customized programs which would allow for such characterization. This system is now in place and we have all software necessary for the characterization of the grains, second phase dispersions and for the tessellation analysis. We are currently working on the methodology for the characterization of the fracture surface profiles.

1. Grains

In our grain structure characterizations we are using a modified linear intercept method described in [3] and [4]*. This method requires the

* These references have been incorporated into this report as Appendix 1 and 2.

constraction of the plots of the average intercept length vs. intercept scan angle (e.g. Appendix 1, Figure 7), and uses these plots to infer the information about grain sizes, shapes, orientations and alignment. The intercept length vs. scan angle data have also been used in the calculation of the coefficients of the functions describing grain dimensions in different directions - this is accomplished through the use of spherical harmonics [5, 6]. The fractions of the recrystallized and unrecrystalized grains have been measured by estimating the area fractions occupied by each grain type.

2. Second Phase Dispersions

The characteristics of the second phase dispersions have been measured using the same method as for grains. The only difference is that in this case the software has to recognize the particles - this is done by painting them with a pre-selected color. These measurements allow then for the estimation of the average values and the distributions of the dispersion sizes, shapes, orientations, area fractions, aspect ratios, etc.

To characterize the distribution of particle spacings, local area fractions and the clustering indexes we used the tessellation method [1, 7-9]. This method allows for the quantification of the minute changes in all above-mentioned characteristics and for the quantification of the nature of the particle clusters, i.e. if they are real or accidental. The reason that we choose to use the area fractions rather than volume fractions in all our characterizationsis is that this quantity is what is actually measured. Consequently it does not contain any error due to the assumption used in the conversions. In addition, since fatigue cracks are usually planar, the measurement on the plane sections are more representative of the microstructural features encountered by the cracks during their growth.

3. Fracture Surface

We are in the process of developing a system for the characterization of the fracture surfaces and fracture profiles. Our characterization method will be based on the measurement of the distributions of the orientations of the line elements along the fracture profiles on the determination of the profile roughness parameter. This will then facilitate calculation of the fracture surface roughness parameter and fractal dimensions [10-14]. The fracture surface profiles will be obtained by sectioning method proposed in ref. [14].

4. Sample Preparation

The sample preparation technique for the optical and scanning electron microscopy examinations described in the Progress Report [2] has been

modified in order to minimize the microstructural damage due to polishing. The surface to be examined is now mechanically ground to a surface finish of 600 grit using wet SiC paper. Next, the samples are polished on a felt wheel with 1 μm and then 0.25 μm diamond paste with ethanol. This new procedure provides a cleaner surface with less particle pull-outs.

The TEM samples were prepared by mechanically grinding slices of the material to approximately 250 μm then punching out 3 mm disks from the thinned material. The disks were dimpled with a jet polisher using a room temperature solution of 10 % nitric acid - 90 % water at a voltage of 25 V. The samples were then perforated using a final polish of 30 % nitric acid - 70 % methanol at -30 °C and a voltage of 18-20 V.

D. Results

1. Grains

Up to date we have compleated characterization of the grains at the surface, quarter depth and center regions on the cross-sections parallel to the plate surface (surface sections) for both pedigree 7050-T7451 plate alloys*. All measurements included quantification of the recrystallization levels and the sizes and shapes of both recrystallized and unrecrystallized grains as well as the subgrains.

The amount of recrystallization changes in both alloys from zero, at the surface, to about 20% in the middle of the plate. However, the degrees of recrystallization is not the same for each pedigree. The area fractions of the recrystallized grains are lower for the old pedigree material, particularly at the quarter depth. The difference is probably due to the different processing conditions for each pedigree. Table 1 lists the percentage of recrystallization for both pedigrees as a function of depth. To our knowledge, these observations are the first recrystallization level data for the 7050-T7451 alloys.

The sizes of the unrecrystallized grains also varied from the surface to the center with the largest grain sizes in the quarter sections of both plates. The new pedigree alloy had a finer grain structure with the sizes between 85 and 150 μm. For the old pedigree the grains were in the 115 to 240 μm range. The trends in the results were not very systematic, Table 1, and the reasons for the scatter is a strong dependance of the unrecrystallized grain sizes on the recrystallization level. It is easy to show that this relation has following form:

---

* The surface sections are designated as longitudinal in Appendix 1.

$$D = D_o \sqrt{1 - f}$$

where D is the measured unrecrystallized grain size, f is the area fraction of the recrystallized grains and D_0 is the starting, i.e. true unrecrystallized grain size. Since there is no recrystallization at the plate surface, then only the surface grains characteristics are those of the true, unrecrystallized grains. The sizes of the unrecrystallized grain at the quarter and middle sections are smaller and reflect both the original unrecrystallized grain size and the recrystallization level.

The variations in the sizes of the recrystallized grains were more consitent, Table 1. These grains were between 25 and 45 μm in size with the larger sizes in the new alloy. In both alloys the grains were larger at the center than in the quarter depth. These trends can be again attributed to the differences in the recrystallization levels.

The subgrains were only present in the unrecrystallized grains. Their average size, for the surface, quarter and middle section was 6.17 μm and their size distribution is shown in Figure 6, Appendix 1. The morphology of the subgrains can be described as the arrays of squares oriented at either 0 or 45° to the rolling direction [3].

The average grain shape characteristics have been measured globally for all three sections. Typical plots used in these measurements are shown in Figure 7, Appendix 1. The aspect ratios obtained from these plots were 1.32 for the unrecrystallized grains, 1.15 for the recrystallized ones and 1.05 for the subgrains. Since these aspect ratios were calculated fom the global average values of the intercept lengths, average aspect ratios based on the data for the individual grain were also estimated and they are listed in Table 2. We have also measured the alignment of the grains with respect to the longitudinal direction [3]. The alignment turned out to be 17.1% for the unrecrystallized grains and 8.9% for the recrystallized ones.

We also used the spherical harmonics method to characterize the grain shapes [5, 6]. This method allows for an easy calculation of the grain diameters in any directions. For instance, for the the ellipsoidal grain approximation the grain diameter, D, in the direction specified by the spherical coordinates α and β is equal to:

$$D(\alpha,\beta) = \frac{1}{N}\{ 1 + \frac{1}{2}(N c - 1) k_2^1 + \frac{3}{2}[\frac{N}{3}(2 a + c) - 1] k_2^2\}$$

where

$$\frac{1}{N} = \frac{a + b + c}{3},$$

$$k_2^1 = 3\cos^2\alpha - 1,$$

$$k_2^2 = \sin^2\alpha \cos 2\beta,$$

a, b and c are averages of the maximum grain lengths in the longitudinal, long transverse and short transverse directions respectively and k_j^i's are

spherical harmonics functions. The preliminary estimates of the values of a, b and c for both pedigrees of 7050-T7451 alloys are given in Table 2.

2. Second Phase Dispersions

i. Pores

SEM examinations showed the presence of two types of pores in both new and old pedigree 7050-T7451 plate alloys. The pores of the first type were usually next to the constituent particles and they appeared as the areas where sections of the constituent particles have been pulled out, as shown in Figure 1. An EDX (Energy Dispersive X-ray) analysis inside them showed either matrix with a high concentration of Cu, Ti, or Si or the presence of a constituent particle. The largest pores of this type tend to contain cracks inside them as seen in Figure 2. Pores of the second type are generally isolated in the matrix and EDX readings showed only matrix composition on their bottom. In most cases these pores were round and their sizes range from 4 μm as in Figure 3 to about 20 μm as in Figure 4.

Quantitative analysis of the porosities on the surface sections had been carried out using the PC-based image analysis system. Results are summarized in Table 3 and they show that the average pore sizes are 7.74 μm for the old and 7.15 μm for the new pedigree alloy. The average pore volume fractions, assumed equal to the area fractions, are 0.074% for the old pedigree and 0.072% for the new pedigree. The volume fraction of the pores for the two alloys are then similar with the slightly lower porosity levels in the new material. These values are higher than those reported by Magnusen et al. [15] for the same materials. We believe that the discrepancies are due to the differences in the sample preparation techniques and, as a result, in the differences in the number of detected pores, pull-outs assumed as pores, etc.

The shapes of the pores were also analyzed and characterized using the methodology described in Appendixes 1 and 2. The average aspect ratios were 1.54 and 1.55 for old and new pedigree alloys respectively which they suggests that the pores in both pedigrees have essentially the same shape.

The spatial distribution of pores have been analyzed using the tessellation method [4]. Figure 5-a shows an example of the tessellation construction for the pores on the surface-section at quarter depth and Table 4 lists all characteristics obtained from the analysis. The most important parameters listed in the Table 4 are local volume fraction, near neighbor distance and nearest neighbor distance - these quantities can be obtained unambiguously only from the tessellations.

To classify the spatial distribution of pores we used following indexes [1]:

$$Q = \frac{\text{Observed Nearest Neighbor Distance}}{\text{Expected Nearest Neighbor Distance}}$$

$$N = \frac{\text{Observed Nearest Neighbor Distance S. Dev.}}{\text{Expected Nearest Neighbor Distance S. Dev.}}$$

where the expected values are calculated by assuming that the pores have random spacial distribution. For the pores in Figure 5-a the expected nearest neighbor distance is 275±144 μm. This gives Q = 1.22 and R = 1.45 which suggests that the distribution of pores in Figure 5-a can be classified as regular with clusters. This is a preliminary result, and we are in the process of accumulating more data to improve the statistics. The problem which we are facing is the need for scanning large areas under high magnification; this assures pore detection and at the same time gives good representation of the pore spatial distribution. Unfortunately this process is very tedious and time consuming as it requires construction of large composite maps from several smaller micrographs.

ii. Constituents

The constituent particles were also investigated using SEM, optical microscopy and EDX techniques. The analysis showed presence of two types of particles in both characterized alloys. The particles of the first type were Al_7Cu_2Fe constituents. They appear as clusters of stringers of various lengths and shapes as shown in Figure 6. The second type of constituents have been identified as $Al_XMg_XSi_X$. These particles also form stringers, but their surfaces were smooth and without clusters as in Figure 7. We also observed number of cracks in the constituents of both types. Although some of the constituents cracking took place during polishing process we have no doubt that the majority of the cracking took place during thermo-mechanical processing of the alloys. This observation is again the first report on the cracked constituents in the 7050-T7451

alloy that we are aware of. We are currently estimating the frequencies of the cracked particles.

The average sizes for both constituent types, measured again on the surface sections, were 8.38 μm for the new pedigree and 8.21 μm for the old pedigree alloy, Table 5. The constituent area fractions were 0.88 % for the old pedigree and 0.65 % for the new one - this change is the most significant improvement in the new 7050-T451 plate alloys which came out from our microstructural analysis. The particle sizes and area fractions obtained in this study were also slightly higher than those reported by Magnusen et al.[15]. As before we attribute these differences to the different sampling techniques.

The analysis of the constituent shapes showed that the particles in the old alloy had aspect ratio 1.75 while for the constituents in the new one it was 1.67, Table 5. This indicates that the constituents are elongated, ellipsoidal in shape and that they are oriented in the rolling direction [4]. This is illustrated in Figures 6 and 7 which show clusters and strings of the constituents along the grain. However, we have also observed instances of isolated, round and slightly oval constituent particles as well.

The spatial distribution of the constituents has been also analyzed using the tessellation method. The results, for the same area as for the pores discussed earlier, are shown in Figure 5-b and they are summarized in Table 5. There are 155 constituents in the test area which corresponds to the expected nearest neighbor spacing of 66.1±34.6 μm. The Q and R values are then 0.93 and 0.92 respectively which suggests that the constituents are clustered.

iii. Precipitates

Preliminary TEM examination of the new pedigree 7050-T7451 alloy showed that the microstructure of precipitate was similar to that of the overaged 7075. The diffraction patterns taken to identify the phases present were identical to those obtained by Park and Ardell [16]. The most common precipitate phases present in the alloy were identified as η', η_1, η_2 and η_4. The precipitate phases inside the grains, Figure 8, are small ranging from 5 to 45 nm in diameters, however the majority of the particles inside the grain are less than 10 nm in size. The precipitates on the grain boundaries are generally larger than the grain precipitates and vary widely in size. Most of the grain boundaries contain smaller precipitates ranging from 20 - 100 nm in size (Fig. 9). A few of the grain boundaries contain larger precipitates which range from 100 - 250 nm (Fig. 10). Examination of the grain boundary precipitates on a boundary inclined to the foil surface showed that the precipitates are hexagonal in

shape, Figure 11. Further study of grain boundary precipitate will have to be done to see if this morphology is common. Precipitate free zones have been also observed, Figure 12, and the measurements of their characteristics are in progress.

E. Modeling

Our theoretical efforts have been limited to the literature survey of the available stochastic life prediction models and to the development of a preliminary Markov chain model. We base our approach on the work by Bogdanov et all [17], Provan [18]and Miller/de los Rios[19-21]. We assume that the distribution of fatigue lives, for the identical loading conditions, depends on the local microstructural fluctuations due to the flaws, varying grain shapes, sizes and orientations, distributions of the second phase particle volume fractions, sizes and spacings, operating crack closure mechanisms, etc.[22-28]. A cumulative effect of all above-mentioned factors is a time to failure distribution curve, with the different microstructural features affecting different parts of that curve. For instance, in aluminum alloys large porosities and non-deformable particles control general shape of the distribution curve and particularly its shape for the short failure times. On the other hand, for the same alloys the precipitates and grain structure control the shape of the tail of the distribution curve. Other factors, most noticeably crack closure, can shift whole curve to the longer or shorter times. We are in the process of evaluating the probabilities of the fatigue crack formation and propagation due to the different microstructural futures present in the 7050 alloys. At the same time we are also working on the correlation of the parameters of the three-parameter Weibull fatigue life distribution curve with the distributions of the microstructural characteristics.

F. Summary of the Technical Accomplishments

Emphasis during the reporting period was on the characterization of the starting microstructures in the "high" and "low" porosity 7050-T7451 commercial plate alloys as a function of the distance from the surface and on the calibration of all quantitative microscopy techniques. Up to date the characterization of the grain structures, constituent particles and pores on the sections parallel to the plate surface have been performed and supplemented with the preliminary TEM studies. In case of the grain structures the measurements have been made using a new variation of the linear intercept method. This techniques is ideally suited for detecting microstructural inhomogeneities. The grain structure measurements show that the recrystallization level changes from zero at the surface to about 20% in the center depth of the plates. The unrecrystallized grain sizes are in the 85 to 240 μm range, while recrystallized grains at the mid-depth are about 40

μm in size. The volume fractions and sizes of both the particles and the pores have been measured using standard methods and tessellation technique. The average sizes of pores are 7.74 μm for old pedigree alloy and 7.15 μm for the new pedigree material with the corresponding area fractions of 0.074% and 0.072%. The sizes of constituent particles are 8.38 and 8.21 μm and area fractions are 0.88% and 0.65% for the old and new pedigree alloys respectively. Preliminary results from the tessellation analysis showed that the pores have regular spatial distribution with clusters. For the constituent particles, the distribution was clustered. A number of the constituent particles have cracks. The measurement of the frequencies of the cracked particles are currently in progress. The observations on the changes in the recrystallization levels from the center to the surface and on the cracked particles are the first observations of this type for 7050-T7451 plate alloys that we are aware of.

G. Future Effort

1. Complete characterization of the 7050-T7451 plate alloys including characterization of the fracture surfaces, damage in the fatigued samples, dislocation structures and textures.
2. Formulate preliminary life prediction models.
3. Start characterization of the 8090 alloys.

H. Publications and Presentations

PUBLICATIONS (Enclosed as Appendix 1 and 2):

1. J. Zhang, A. J. Luevano and M. A. Przystupa, "Quantitative Analysis of Heterogeneous Grain Structures on Plane Sections", accepted for publication in Scipta Metallurgica et Materialia.

2. J. Zhang, A. J. Luevano and M. A. Przystupa, " Theoretical Models for Quantitative Analysis of Grain and Particle Shapes", in preparation.

PRESENTATIONS (Abstracts enclosed as Appendix 3):

1. M. A. Przystupa, J. Zhang, A. J. Luevano, "The Effect of Microstructural Fluctuations on the Fatigue Life Distributions in Aluminum Alloys", to be presented during the TMS Annual Meeting in San Diego, March 1-5, 1992.

2. A. J. Luevano, J. Zhang and M. A. Przystupa, "Precipitate Phase Identification and Grain Boundary Precipitate Characterization of the Aluminum Alloys 7050 in the T7 Temper", to be presented during the TMS Annual Meeting in San Diego, March 1-5, 1992.

3. J. Zhang, A. J. Luevano and M. A. Przystupa, "Quantitative Evaluation of Grain Sizes and Shapes of Aluminum 7050 Alloys", to be presented during the TMS Annual Meeting in San Diego, March 1-5, 1992.

I. References

1. M. A. Przystupa, ONR Proposal Titled "Development of the Microstructure Based Stochastic Life Prediction Models", Dept. of Material Sci. and Eng., UCLA, November 1990.
2. M. A. Przystupa, Progress Report, ONR Grant No: N00014-91-J-1299, UCLA, June 1991
3. J. Zhang, A. J. Luevano and M. A. Przystupa, "Quantitative Analysis of Heterogeneous Grain Structures on Plane Sections", accepted for publication in Scripta Metallurgica and Materialia.
4. J. Zhang, A. J. Luevano and M. A. Przystupa, Theoretical Models for Quantitative Analysis of Grain and Particle Shapes", in preparation.
5. J. A. Szpunar and B. K. Tanner, J. of Mater. Sc., vol. 19, p. 3254, 1984.
6. H.-J. Bunge, "Texture Analysis in Materials Science", Butterworth & Co 1982.
7. P. J. Wray, O. Richmond, H. L. Morrison, Metallography, vol. 16, p. 39, 1983.
8. W. A. Spitzig, J. F. Kelly, O. Richmond, Metallography, vol. 18, p. 235, 1985.
9. M. A. Przystupa, "Application of the Dirichlet Tessellation Procedure for Microstructure Characterization", Progress Report DM16-1, Alcoa Laboratories, Alloy Technology Div., 1985
10. M. Coster and J. L. Chermant, Int. Metals Rev., vol. 28, p. 228, 1983.
11. S. M. El Soudani, Metallography, vol. 11, p. 247, 1978.
12. E. E. Underwood, "Recent Advances in Quantitative Fractography", in Fracture Mechanics: Microstructure and Micromechanisms, ed. by S. V. Nair et al., p. 87, ASM International, Metals Park, Ohio, 1989.
13. A. M. Gokhale and E. E. Underwood, Met. Trans. vol. 21A, p. 1192, 1990
14. A. M. Gokhale and W. J. Drury, Met. Trans., vol. 21A, p. 1201, 1990
15. P. Magnusen, A. J. Hinkle, R.J. Bucci, R. L. Rolf and D. A. Lukasak,"Methodology for the Assessment of Material Quality Effects on Airframe Fatigue Durability," Alcoa Lab. Technical Report, No. 57-89-40.
16. J. K. Park and A. J. Ardell, Acta Metall. vol. 34, No. 12, pp. 2399-2409, 1986 .
17. J. L. Bogdanoff and F. Kozin, "Probabilistic Models of Cumulative Damage", John Willey & Sons, 1985.
18. J. W. Provan ed., "Probabilistic Fracture Mechanics and Reliability", Martinus Nijhoff Publishers, 1987.

19. K. J. Miller and E. R. de los Rios eds., "Short Fatigue Cracks", Inst. Mech. Engrs, London 1986.
20. Z. Sun, E. R. de los Rios and K. J. Miller, Fatigue Fract. Engng Mater. Struct., vol. 14, p. 277, 1991
21. Z. S. Wang, K. J. Miller, M. W. Brown and E. R. de los Rios, Fatigue Fract. Engng Mater. Struct., vol. 14, p. 351, 1991
22. W. L. Morris and M. R. James, "Statistical Aspects of Fatigue Due to Alloy Microstructure", in Fatigue Mechanisms: Advances in Quantitative Measurement of Physical Damage, ed. by J. Lankford et al., STP 811, ASTM STP 811, ASTM, 1983.
23. A. K. Zurek, M. R. James and W. L. Morris, Met. Trans, vol. 14A, p. 1697, 1983.
24. T. Lin, A. G. Evans and R. O. Ritchie, Met Trans, vol. 18A, p. 641, 1987.
25. J. Gill Sevillano, Texture and Microstructure, vol. 12, pp. 77-87, 1990.
26. K. S. Chan and J. Lankford, Acta Met, vol. 36, p. 193, 1988.
27. Fatigue Fract. Engng Mater. Struct., vol. 14, 1991 (Small Cracks Issue)
28. Mater. Sci. Eng., vol. A103, 1988 (Issue with papers presented at the Workshop on the Mechanics and Physics of Crack Growth: Application to Life Prediction)

J. Tables and Figures

Table 1. Characteristics of Grains in Al 7050-T7451 Alloys

	Surface	Quarter			Center		
	d (μm) unrecrystallized	d (μm) unrecrystallized	d (μm) recrystallized	% recrystallization	d (μm) unrecrystallized	d (μm) recrystallized	% recrystallization
Old Pedigree	191.22	239.34	24.18	1.0	114.45	37.85	17.5
New Pedigree	85.26	131.05	43.77	21.8	148.55	45.03	22.2

Table 2. Characteristics of the Grain Shapes and Orientations in the Middle Sections of the 7050-T7451 Plate Alloys

Alloy Pedigree	Recryst. Level	Aspect Ratio	$\Omega_{1,2}$% Alignment	Ellipsoidal		
				a	b	c
New	Recryst.	1.960	9.71	35.58	42.89	50.14
	Unrecr.	2.436	29.87	165.84	78.45	130.92
Old	Recryst.	2.096	26.74	41.44	58.82	37.38
	Unrec.	2.278	30.54	163.18	68.29	115.48

Table 3. Characteristics of the pores and constituents in the 7050-T7451 alloy

	Pores			Particles		
	Area %	Average d (μm)	Aspect Ratio	Area %	Average d (μm)	Aspect Ratio
155 Old Pedigree	0.074	7.74 ± 3.00 (n=114)	1.54	0.88 ± 0.1	8.38 ± 3.17 (n=1014)	1.75
157 New Pedigree	0.072	7.15 ± 4.89 (n=93)	1.55	0.65 ± 0.3	8.21 ± 2.43 (n=1047)	1.67

(n is the total number of pores or particles measured.)

Table 4. Results of the Tessellation Analysis for the Porosities in the New Pedigree 7050-T7451 Plate Alloy (Surface Section, Quarter Depth)

	Average	Minimum.	Maximum	St. Dev.	Geom.Av.	Median
Near-Neighbor. (μm)	689.	42.7	1150	283.	578.	782.
Nearest-Nbr. (μm)	336.	42.7	570.	209.	241.	373.
Local V.F. %	.053	.021	.112	.034	.045	.037
Particle Area (μm^2)	161.	54.6	400.	125.	126.	127.
Cell Area (mm^2)	.311	.120	.550	.140	.283	.269
Particle Width (μm)	9.29	1.25	19.4	5.37	7.52	9.08
Particle Len. (μm)	13.0	7.62	21.9	5.02	12.1	12.9
Part. Aspect Ratio	2.39	1.03	11.2	3.33	1.62	1.25
Neighbor Pos. (°)	32.7	-180.	180.			
Particle Orient. (°)	90.0	.000	180.			
Cell Sides No.	4.89	3.00	15.0			

Table 5. Results of the Tessellation Analysis for the Constituent Particles in the New Pedigree 7050-T7451 Plate Alloy (Surface Section, Quarter Depth)

	Average	Minimum	Maximum	St. Dev.	Geom.Av.	Median
Near-Neighb. (μm)	144.	15.4	418.	77.3	121.	154.
Nearest-Nbr. (μm)	61.4	15.4	170.	31.9	53.9	55.1
Local V.F. %	1.42	.042	15.6	2.19	.752	.760
Particle Area (μm^2)	180.	9.10	1860	243.	112.	109.
Cell Area (mm^2)	.0180	.00184	.1480	.0142	.0150	.0160
Particle Width (μm)	7.19	2.70	23.0	2.78	6.78	6.82
Particle Len (μm)	11.0	6.75	42.3	5.12	10.3	9.47
Part. Aspect Ratio	1.58	1.00	4.30	.498	1.51	1.49
Neighbor Pos.(°)	6.63	-180.	180.			
Particle Orient. (°)	88.3	.000	180.			
Cell Sides No.	5.77	3.00	15.0			

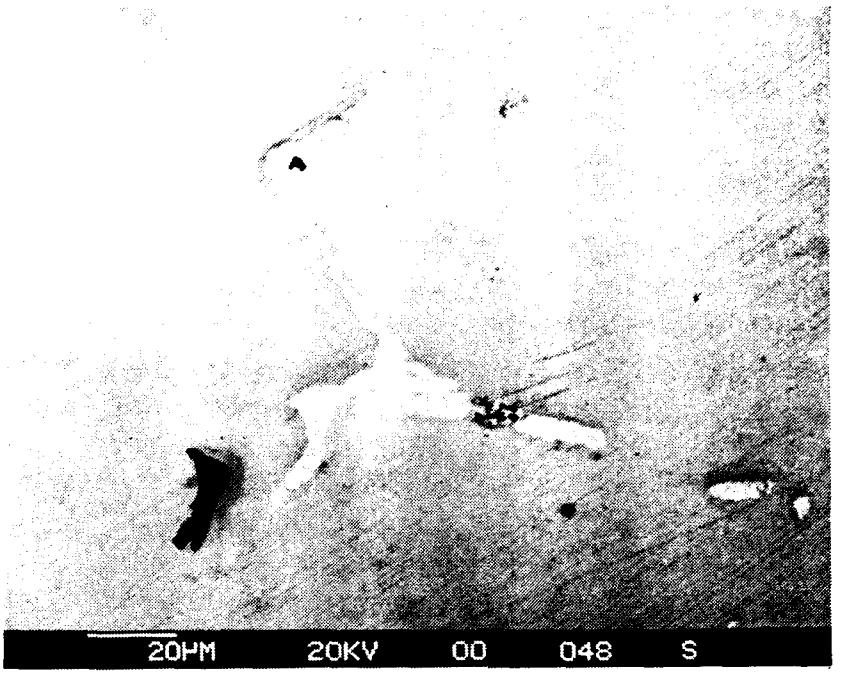

Figure 1. A typical pore associated with the broken constituent particle.

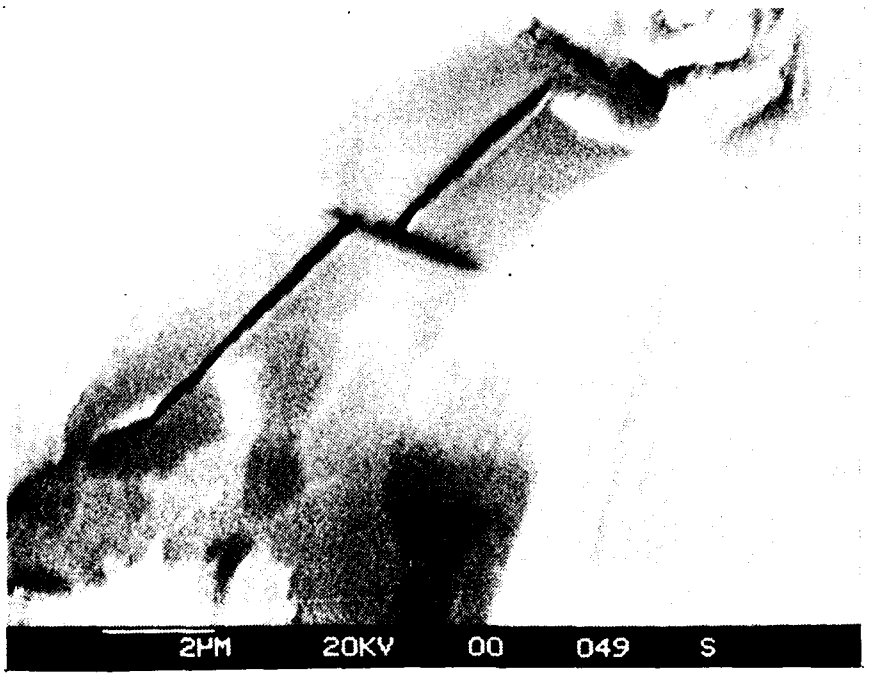

Figure 2. A close-up of the inside of the pore with a broken constituent particle on the bottom.

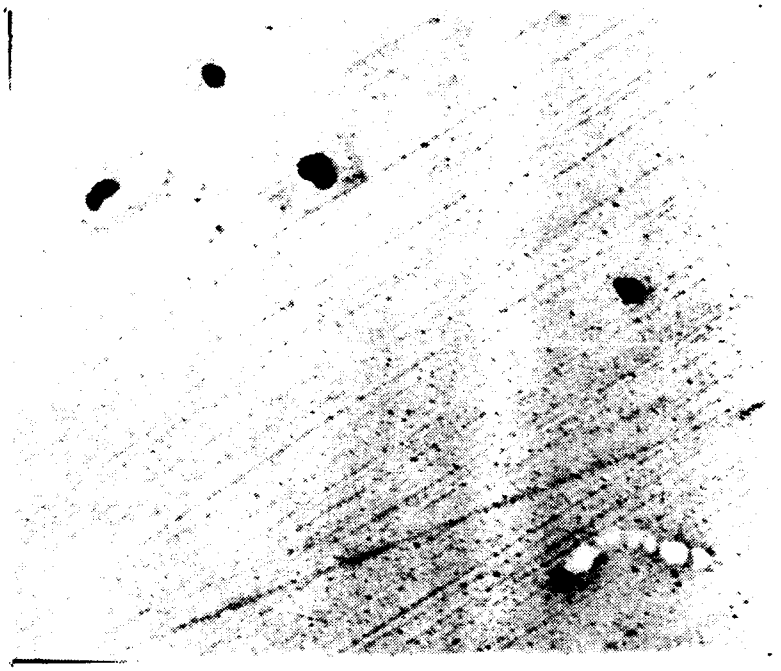

16.7 μm

Figure 3. A typical small isolated pore.

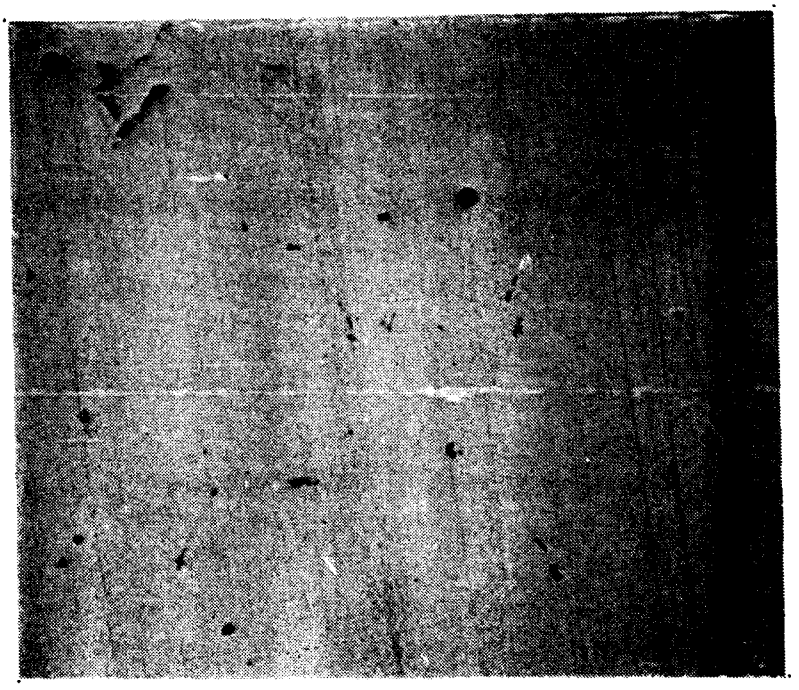

200 μm

Figure 4. A typical large isolated pore.

(a)

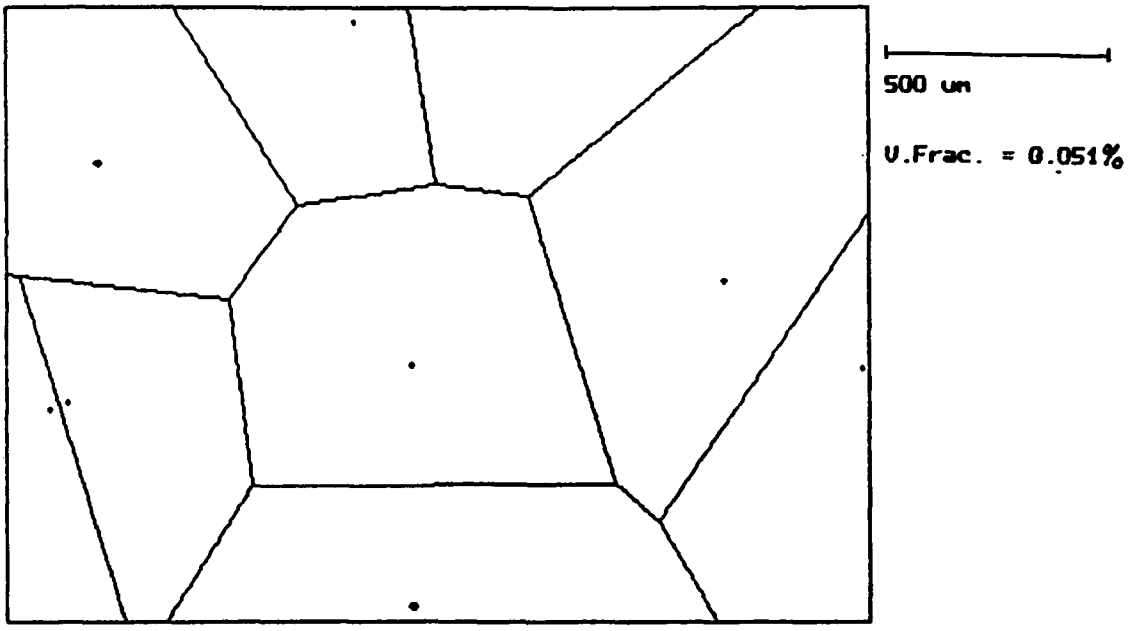

(b)

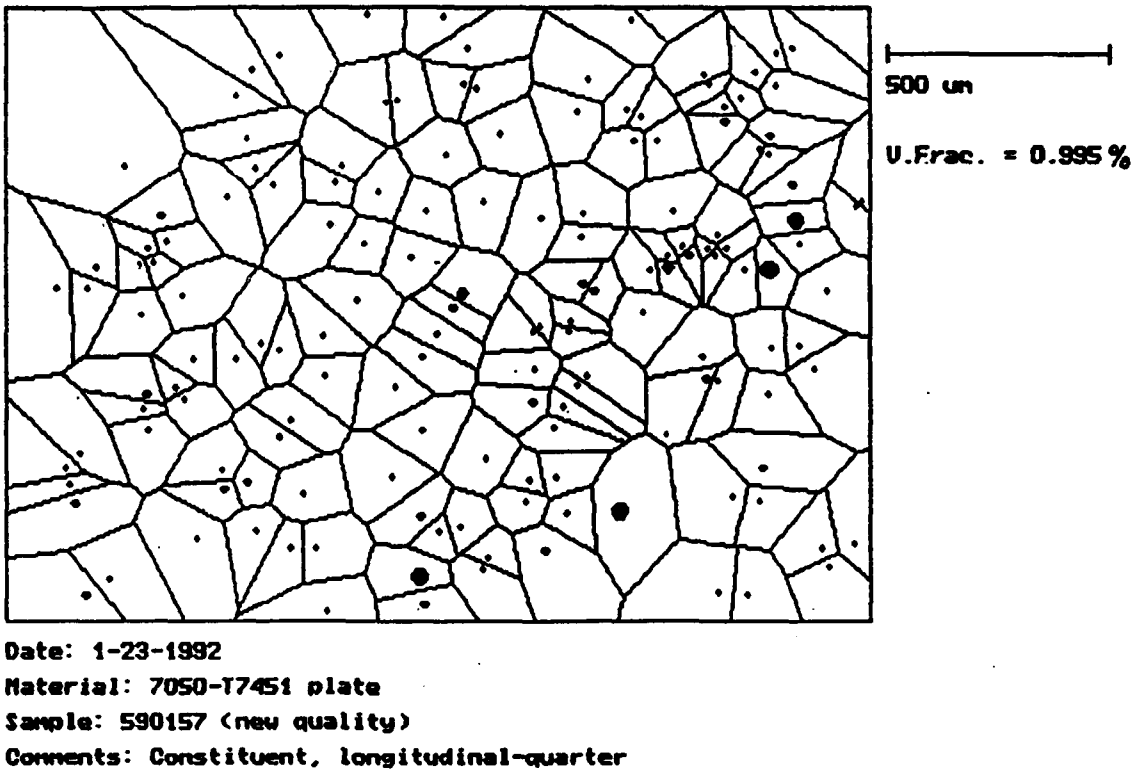

Figure 5. An example of the tessellation construction for (a) porosities (regular distribution with clusters) and (b) constituent particles (clustered distribution) - the area is the same for both a and b. (7050-T7451 alloy, plane parallel to the surface, quarter depth)

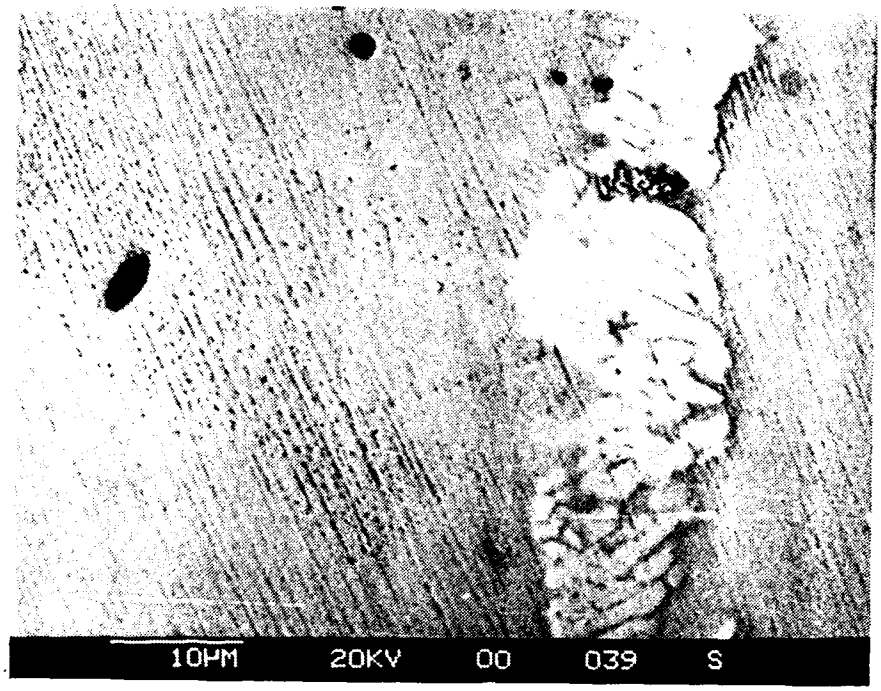

Figure 6. A cluster of stringers of the Al_7Cu_2Fe constituents.

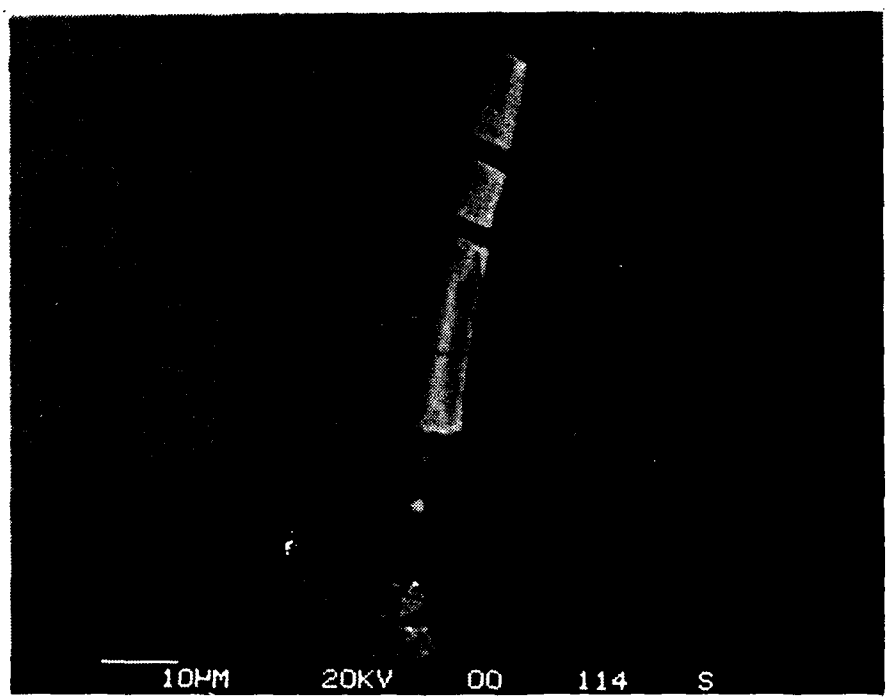

Figure 7. Characteristic stringer of the constituent of the $Al_xMg_xSi_x$ type.

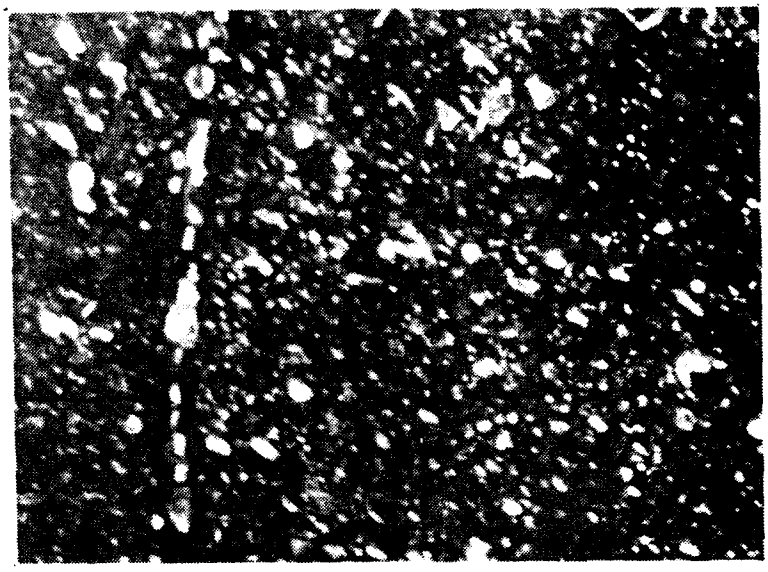

150 nm

Figure 8. Precipitates inside grains.

80 nm

Figure 9. Precipitates on grain boundary.

385 nm

Figure 10. Large precipitates on grain boundary.

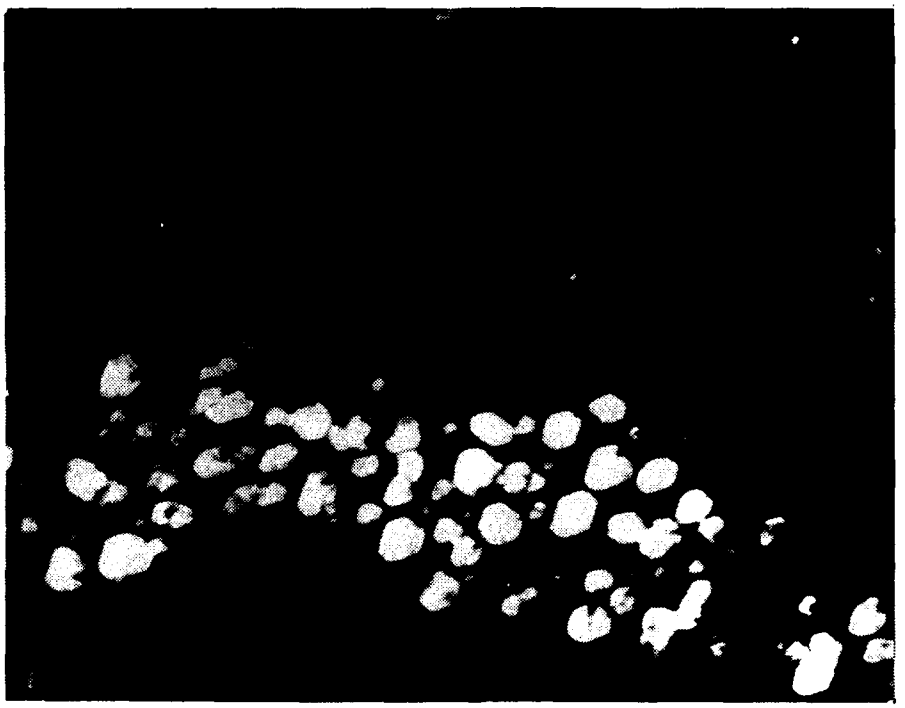

150 nm

Figure 11. Dark field image of precipitates on boundary inclined to foil surface.

Figure 12. Bright field image showing precipitate free zone.

APPENDIX 1

QUANTITATIVE ANALYSIS OF HETEROGENEOUS GRAIN STRUCTURES ON PLANE SECTIONS

Jimin Zhang, Annetta J. Luévano and Marek A. Przystupa

Department of Materials Science and Engineering, University of California
Los Angeles, CA 90024, USA

Introduction

Since most of the engineering materials have heterogeneous grain structures, their complete quantitative description must include not only the average values of grain sizes but also contain some quantification of their shapes and orientations. The standard procedure used in these characterizations usually involves measurement of the linear intercepts on the plane sections and then conversion of the intercept values to the grain sizes, shape factors, etc. [1, 2]. Depending on the idealized grain model used in the conversion, one obtains either three or two dimensional grain descriptions, and the variation of the grain structure is described either by the standard deviations or by the distribution plots.

Among all grain characteristics the shape is the most elusive. The prevailing approach in its characterization is to use arbitrarily defined shape factors. The quantity most often used for this purpose is the ratio of the grain or particle area to the square of its perimeter [3]. Other definitions of shape factor include ratios of the feature area to the area of a circumscribed circle or rectangle, aspect ratios of the circumscribed rectangle and ratios of variously defined length and width values [4, 5]. All these descriptions have been extensively discussed by Underwood [1] and DeHoff et al. [2].

In this work we are concerned with the measurements of the characteristics of heterogeneous grain structures on the plane sections, that is with the measurement of the parameters which are important in the modeling of mechanical properties or in characterizing the extent and nature of the prior thermo-mechanical processing. Our approach is based on the measurement of the linear intercepts on the plane sections and uses plots of the average intercept length vs. intercept scan angle to characterize structural inhomogeneities. These plots have been already proven useful in characterizing oriented grain structures [6]. In what follows we first test the sensitivity of the method by deriving theoretical relationships between the average intercept length and the intercept scan angle for simple geometrical shapes. We then show how to obtain the information about the grain size, aspect ratio and shape from the intercept length vs. angle plots. Finally the versatility of the method is illustrated in the analysis of the grain structure of the 7050-T7 aluminum alloys with partially recrystallized structure.

Theoretical Models

Let us start from defining an average intercept length, $L_i(\alpha)$, as an average of all intercepts obtained from a set of parallel test lines drawn at angle α through a two dimensional object. The relations between these averages and the scan angles are easy to derive and they are compiled, for

simple geometrical shapes, in Table I [7]. Figure 1 shows variation of the normalized average intercept lengths, d ($= L_s(\alpha)/L_{s,max}$) vs. α for a circle, selected regular polygons and a rectangle ($\alpha = 0$ for the direction corresponding to the maximum average intercept length, $L_{s,max}$). The curves have some interesting features. First, the average intercept length is a periodic function of α with a period $2\pi/n$ (n is the number of sides of a regular polygon). Second, it is possible to show that the amplitudes of these curves decrease with n and that they are proportional to $cos(\pi/n)$ [7]. Finally, for a rectangle the value of d at 90° is equal to the aspect ratio. This property is further illustrated in Figure 2 which shows curves for rectangles with different aspect ratios, and in Figure 3 which shows similar plots for a circle and ellipses (b and a are either height and width or minor and major axes respectively). In the case of ellipses, as for rectangles, the normalized average intercept length d changes with the scan angle and the aspect ratios can be also deduced from the plots [7]. The d vs. α curves are then ideal for finding about the average shape and the aspect ratios of the measured features.

Another useful property of the d vs. α curves is that they can be used to calculate the global average of all intercept lengths for all angles, L_g, which is as a measure of the object size. This average is equal to:

$$L_g = \frac{\int_0^{\alpha_p} H(\alpha) L_s(\alpha)\, d\alpha}{\int_0^{\alpha_p} H(\alpha)\, d\alpha} \qquad (1)$$

or, equivalently, to:

$$L_g = \frac{\pi A}{L_p} \qquad (1a)$$

where α_p is the curve period, $H(\alpha)$ is a projection of the measured shape on the direction perpendicular to the scan lines, A is figure area and L_p its perimeter [1]. The d vs. α plots also suggest that the shape index, SI, (defined as the normalized area under the curve):

$$SI = \frac{1}{\alpha_p} \int_0^{\alpha_p} d\, d\alpha \qquad (2)$$

will be a sensitive measurement of the differences in the grain shapes. Indeed, it is equal to 1 for a circle and decreases to 0.9485 for regular octagon, to 0.9085 for hexagon and to 0.7936 for square. For the rectangles and ellipses SI increases with b/a and for $b/a = 1$ it reaches the values for square and circle respectively. The d vs. α curves for more complex shapes, such as elongated polygons with different number of sides, have identical properties and can be also used in the characterizations of grain structures [7].

Although thus far L_g and SI have been defined for specific shapes, they can be also used for characterizing either regular grids of simple figures or oriented grain structures modeled as polygons, ellipses, etc. In these cases the d vs. α plots have the same characteristics as a plot for a single element if the structure is perfectly aligned. If grains have the same shapes but are not aligned, then their d vs. α curves exhibit phase difference and integrations in Eqs. 1 and 2 have to be carried out from 0 to π. For such structures the value of L_g remains the same, but the SI will now reflect both the grain shape and the alignment and it will be greater than that for a corresponding perfectly aligned structure. In the limiting case of randomly oriented identical non-spherical

grains, the d vs. α is a horizontal line and the SI is equal to one. For such random structures the grain shape characteristics have to be measured individually and they can not be obtained from the globally measured intercept values.

In order to fully characterize the grain structure, one also needs to quantify grain orientation or alignment. The simplest parameter for this purpose is the ratio of the average intercept lengths for 0 and 90°, i.e. $L_3(\alpha=0)/L_3(\alpha=90)$. A more precise parameter, which we are going to use in this work, is the ratio of the total length of oriented lines to the total length of all lines, $\Omega_{1,2}$. This ratio was introduced by Saltykov[6] and for our case is equal to [1, 6]:

$$\Omega_{1,2} = \frac{L_3(\alpha=0) - L_3(\alpha=90)}{L_3(\alpha=0) + 0.571\, L_3(\alpha=90)} \qquad (3)$$

The value of $\Omega_{1,2}$ is zero for random structure and approaches one for structure with highly oriented and elongated grains.

Experimental

The material used to test the proposed method was partially recrystallized aluminum 7050-T7 plate alloy. The metallographic specimens used in the analysis were prepared by grounding on 600 grit sandpaper, and then polished using 9 μm alumina powders and finally 3 μm diamond paste. All samples were etched using Keller's 3A etchant for 20 to 45 seconds to reveal grain and subgrain boundaries respectively. Several photographs at magnifications 100X and 500X have been taken to study the grain structures. These photographs were scanned and saved as computer image data files for the analysis by a linear intercept program. The program automatically measures intercept lengths using scan angles from 0 to 180° from the horizontal axis, and then calculate average intercept lengths, shape indices, aspect ratios, size distributions, etc. All calculations take several minutes on a PC-based system.

Results and Discussion

The 7050-T7 alloy is an ideal material to test the proposed method. It has both recrystallized and unrecrystallized grains and in addition all unrecrystallized grains have networks of well defined subgrains. Although the alloy shows different grain structures on all three L, S and T sections, only grains and subgrains on longitudinal planes were characterized in this study. Figures 4 and 5 show representative microstructures used in the analysis. The micrographs were taken from the middle, Figure 4, and top, Figure 5, sections of the plate. Figure 4 shows evidences of partial recrystallization, while recrystallized grains are absent in Figure 5. This indicates that the fraction of the recrystallized grains changes from the top of the plate to the middle (Note that sample in Figure 5 was etched for a short time to reveal grain boundaries only).

Both recrystallized and unrecrystallized grains and subgrains have different characteristics and have been measured separately to evaluate the sensitivity of the proposed method. The measurements showed that the average intercept length, L_3, was 97.6 μm for the unrecrystallized grains, 72.6 μm for the recrystallized grains and 6.9 μm for the subgrains. Figure 6 shows distributions of the intercept lengths: they differ not only in their averages but also in the scatter. The distribution for the subgrains is very narrow and well defined while those for the recrystallized and unrecrystallized grains have considerable spread. The interesting feature of the distribution for unrecrystallized grains is presence of two diffused maxima which give rough estimate of the average grain width and length.

Figure 7 shows d vs. α curves for all three types of grains. The shape indices, *SI*, are 0.811 and 0.886 for the unrecrystallized and recrystallized grains respectively and 0.920 for subgrains. As expected, the *SI* for the unrecrystallized grains is the smallest, which indicates that they are the most elongated. This is further supported by the lowest d_m value for these grains. A surprisingly high *SI* and 45° periodicity of the curve for subgrains can be attributed to the preferential alignment of subgrain boundaries at either 0 or 45°. This results in a structure which can be approximated as two arrays of squares rotated by 45°. Such a structure has shape factor 0.930, which is very close to the observed value. It should be again emphasized that in addition to representing the normalized average intercept lengths the *SI* values also characterize the randomness of the structure - the higher the value, the more random, or isometric, is the structure. Consequently, in order to characterize the orientation and average grain shape in the isometric microstructures, it is necessary to calculate the *SI* for *each* grain individually and then use obtained data to deconvolute the global *SI* into the orientation and shape components [7].

Also, the aspect ratio d_l/d_m was 1.324 for the unrecrystallized grains and 1.154 for the recrystallized ones. The reason for the difference is that the recrystallized grains are more equiaxed. The aspect ratio for subgrains was the smallest and equal to 1.054.

As to the grain alignment, the orientation parameter $\Omega_{1,2}$ was 17.1% for the unrecrystallized grains, 8.9% for the recrystallized ones and 3.3% for the subgrains. These values again indicate that both subgrains and recrystallized grains had practically no preferred orientation while unrecrystallized grains were oriented only slightly. This is in agreement with the finding based on the d vs α curves which further indicates the consistency of the method and its usefulness in precise characterization of the grain structures.

Conclusions

1. Theoretical models for calculating the change of the average intercept lengths with the scan angles for simple geometrical shapes have been developed. These models can be used to study relations between various shapes and their average intercept lengths, aspect ratios and shape indices. They can be also applied to the characterization of the heterogeneities in the partially aligned microstructures of single or multiphase alloys and composites.

2. The grain structures of partially recrystallized aluminum 7050-T7 alloy have been characterized using proposed methodology. Both recrystallized and unrecrystallized grains and subgrains have been studied. The method allowed for the quantification of minute differences in sizes, shapes and preferred orientation of all grain and subgrain types.

3. The plots of average linear intercept vs. scan angle provide quantitative information on grain sizes, shapes and orientation needed in the modeling of mechanical properties and/or in the characterization of the extent of thermo-mechanical processing. Since these plots contain information about both grain shapes and orientation, they are most useful for quantifying differences between partially aligned structures. A more detailed description of the individual grain shapes is needed for the characterization of the structures of randomly oriented grains.

Acknowledgment

The authors are grateful to Alcoa Laboratories for providing us with the material and to the Office of Naval Research for their support under Grant No. N00014-91-J-1299 of which Dr. A. K. Vasudevan is the program manager.

References

1. E. E. Underwood, ***Quantitative Stereology***, Addison-Wesley Publishing Company, Reading, Massachusetts, pp196-197, 1970.
2. R. T. DeHoff and F. N. Rhines, editors. : ***Quantitative Microscopy***, McGraw-Hill Book Company, New York, NY 10036, USA (1968).
3. S. Miyata and M. Kikuchi, "Quantitative Analysis of the Graphite Structure in Cast Iron by a Statistical Method," ***Trans. Natl. Res. Inst. Met.***, vol. 16, No. 3, 1974, pp 25-31.
4. T. L. Capeletti and J. R. Hornaday, "Nodular Iron Shape Factor A New Approach to Quantifying Graphite Morphology," ***Trans. Am. Foundarymen's Soc.***, vol. 82, 1974, pp59-64.
5. H. H. Hausner, "Characterization of the Powder Particle Shape," ***Planseeber. Pulvermetall.***, vol. 14, 1966, pp75-84.
6. S. A. Saltykov, ***Stereometric Metallography***, Second edition, Moscow: Metallurgizdat (1958).
7. J. Zhang, A. J. Luévano and M. A. Przystupa: "Theoretical Models for Quantitative Analysis of Grain and Particle Shapes" Submitted to ***Materials Characterization***.

Table 1. Compilation of Expression for Average Intercept Lengths for Selected 2-D Figures

Form	Average Intercept Length $L_2(\alpha)$	Period
Circle:	$\frac{\pi a}{2}$	-------
Square:	$\frac{a}{\cos\alpha+\sin\alpha}$	$\pi/2$
Rectangle:	$\frac{a}{\cos\alpha+\frac{a\sin\alpha}{b}}$	$\pi/2$
Hexagon:	$\frac{\frac{3}{2}a\cos(\frac{\pi}{6})}{\cos(\frac{\pi}{6}-\alpha)}$	$\pi/3$
Octagon	$\frac{2a(1+\sqrt{2})}{\sin\alpha+(1+\sqrt{2})\cos\alpha}$	$\pi/4$

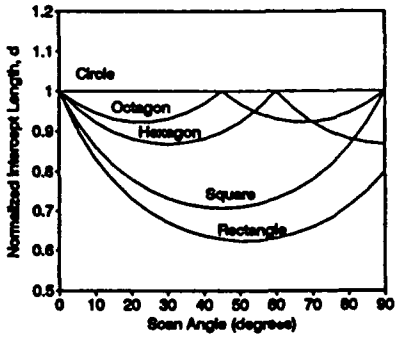

Fig. 1. Normalized intercept length d as a function of α for circle, octagon, hexagon, square and rectangle.

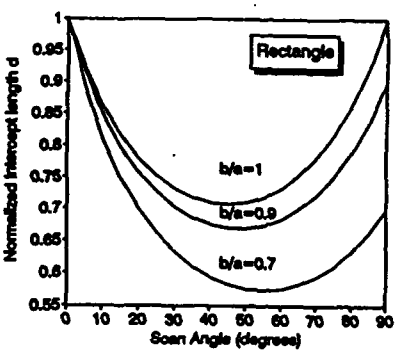

Fig. 2. Normalized intercept length d as a function of α for rectangles with different aspect ratios b/a.

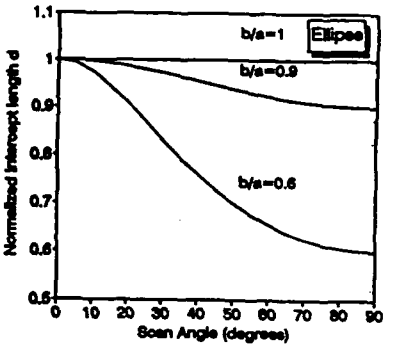

Fig. 3. Normalized intercept length d as a function of α for ellipses with different major and minor axis ratios b/a. (a is constant for all three curves).

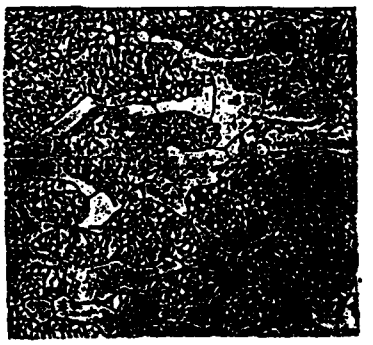

Fig. 4. Microstructure of Al 7050 near middle section of the plate showing a mixture of unrecrystallized and recrystallized grains.

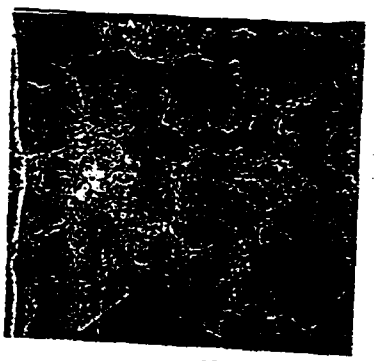

Fig. 5. Microstructure of Al 7050 near top section of the plate showing unrecrystallized grains only.

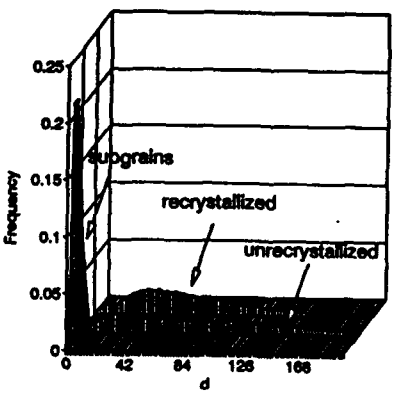

Fig. 6. Size distributions of different grains: recrystallized, unrecrystallized and their subgrains.

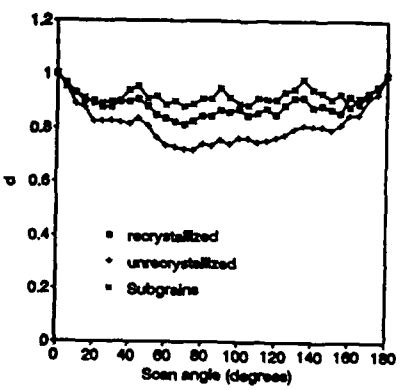

Fig. 7. Normalized intercept length vs. scan angle for the different grains. Overall shape indices are the areas under the curves.

APPENDIX 2 (Draft)

Theoretical Models for Quantitative Analysis of Grain and Particle Shapes

Jimin Zhang, Annetta J. Luevano and Marek A. Przystupa

Department of Materials Science and Engineering, University of California, Los Angeles, CA 90024, USA

INTRODUCTION

Mechanical properties of crystalline materials depend strongly upon the sizes of grains and/or second phase particles. However, for heterogeneous materials, such as those with varying grain sizes, two-phase aggregates and composites, other variables such as size distribution, aspect ratio, shape factor and local volume fraction play important roles in controlling their mechanical properties. It is therefore necessary to characterize both the sizes and the shapes of grains and/or particles in order to correlate the microstructure and the mechanical behavior of the materials. Since analysis of such microstructure normally involves extensive work, methodology combining the mathematical models and computerization of quantitative metallography has very practical significance.

This work extends the analysis of the shape index based on the linear intercept method introduced by Zhang et al[1]. The polar plots of d-α curves and the shape indices for regular polygons are treated here to complete the theory. Various mathematical models for elongated polygons are proposed to describe the different shapes commonly encountered in engineering materials. It is also shown how the global shape index mentioned in our previous paper[1], can be deconvoluted into shape and orientation components; an example is given in this paper. A new parameter to describe orientation of the grains structures is also defined and used to characterize the selected microstructure in Al 7050 alloy. These models provide theoretical bases for automation of quantitative analyses of shapes, sizes and orientations of the grains and/or particles. In addition, the method has potential applications in fracture profile analysis [2] and other image-related areas.

THEORETICAL MODELS

1. Intercept Length

The average intercept length $L_2(\alpha)$ of a two dimensional shape at a scan angle α can be defined as

$$L_2(\alpha) = \frac{A}{H(\alpha)} \qquad (1)$$

where $L_2(\alpha)$ is the average value of all the intercept lengths at given scan angle α, A is the area of the shape and $H(\alpha)$ is the tangent height at α, i. e. a projection of the measured shape on the direction perpendicular to the scan lines. Since A is a constant for a given shape, the $L_2(\alpha)$ is only function of tangent height of the shape. If average value of L_{II} over all the scan angles are considered, then

$$L_{II} = \sum_{1}^{n} \left(\frac{A}{H_i(\alpha)}\right) \frac{H_i(\alpha)}{\sum_{1}^{n} H_i(\alpha)} \qquad (2)$$

$$L_{II} = \frac{A\,n}{\sum_{1}^{n} H_i(\alpha)} \qquad (3)$$

Substituting $n = \pi/\Delta\alpha$ into (3) gives

$$L_{II} = \frac{\pi A}{\Delta\alpha \sum_{1}^{n} H_i(\alpha)} \qquad (4)$$

and

$$L_{II} = \frac{\pi A}{\pi \int_{0} H(\alpha)\, d\alpha} \qquad (5)$$

In case of convex shapes, $\int_{0}^{\pi} H(\alpha)\, d\alpha = L_p$, thus[3]

$$L_{II} = \frac{\pi A}{L_p} \qquad (6)$$

where L_p is the perimeter of the measured feature.

The expression for the intercept length for triangle, rectangle, ellipse and regular polygons are derived first using Eq. (1). These forms are the simplest geometric shapes (square and circle can be viewed as special cases for rectangle and ellipse respectively) and will be used as the bulding blocks for more complicated shapes.

Triangle is the first geometric shape to be analyzed due to its simplicity. For an equilateral triangle with side length a, the relation between $L_2(\alpha)$ and α is:

$$L_2(\alpha) = \frac{a \sin\frac{\pi}{3}}{2 \sin(\frac{\pi}{3}+\alpha)} \qquad (7)$$

Once the formulae for triangles are obtained, they can be used as elements for the more complicated shapes. For instance, a rectangle can be viewed as a combination of two triangles and a hexagon as of six. For a shape consisting m simple shapes, the formula for the intercept length $L_2(\alpha)$ is

$$L_2(\alpha) = \frac{\sum_{0}^{m} d_i H_i(\alpha)}{H(\alpha)} = \frac{\sum_{0}^{m} A_i}{H(\alpha)} \qquad (8)$$

The application of equation (8) is quite general because many complicated shapes can be formed by subtracting one shape from another. For example, a ring can be viewed as a larger circle minus a concentric smaller one; in these cases the areas of inner shapes is negative. Consequently, Eq. (8) enables one to characterize any concave shapes which can be decomposed into several simple ones.

Another important feature of Eq. (8) is that the position of inner shape (A_i is negative) has no effect at all on the value of $L_2(\alpha)$. For instance, if Eq. (8) is applied to a ring, then the value of $L_2(\alpha)$ would be

the same no matter the two circles are concentric or not. Furthermore, if the shape is convex, Eq. (8) can be further extended to the average intercept length

$$L_{II} = \frac{\pi\sum_{0}^{m} d_i H_i(\alpha)}{L_p} = \frac{\pi\sum_{0}^{m} A_i}{L_p} \qquad (9)$$

The intercept length $L_2(\alpha)$ for a rectangle is obtained by using Eq. (8) as

$$L_2(\alpha) = \frac{ab}{a\sin\alpha + b\cos\alpha} \qquad (10)$$

where a and b are the width and height of the rectangle respectively. Eq. (10) becomes the formula for a square when $a = b$, i. e.

$$L_2(\alpha) = \frac{a}{\sin\alpha + \cos\alpha} \qquad (11)$$

Ellipses are another group of shapes studied in this work because of its potential application in the microstructural characterization. To develop expression of $L_2(\alpha)$ for an ellipse, the tangent height, $H(\alpha)$, in Eq. (1) is first calculated as:

$$H(\alpha) = 2\sqrt{\frac{b^2 + a^2\tan^2\alpha}{1+\tan^2\alpha}} \qquad (12)$$

where a and b are the major and minor axes of the ellipse. The intercept length $L_2(\alpha)$ for ellipse is, after substituting Eq. (12) with $A = \pi ab$ into Eq. (1)

$$L_2(\alpha) = \frac{\pi ab}{2}\sqrt{\frac{1+\tan^2\alpha}{b^2 + a^2\tan^2\alpha}} \qquad (13)$$

The plot of d, which is normallized $L_2(\alpha)$, vs. α for ellipse with different ratios of b/a is shown on Figure 1. It is interesting to note that the normallized average intercept length d is a function of both the scan angle and the ratio of minor to major axes, i. e. b/a. Since $d_{\alpha=0} = \frac{\pi a}{2}$; and $d_{\alpha=90} = \frac{\pi b}{2}$; The aspect ratio defined by $d_{\alpha=0}/d_{\alpha=90}$ is the same as the ratio of a/b.

Since Eq. (13) is true for the shapes varying from a perfect circle, where $a = b$, to any ellipse with large aspect ratios, it can be used to characterize any shapes which are ellipses-like.

Eq. (1) can be now applied to obtain the intercept lengths for regular polygons in general. For a regular polygon with an even number of side n, the area of the polygon is:

$$A = \frac{na^2}{4\tan(\frac{\pi}{n})} \qquad (14)$$

where a is the side of the polygon.

The intercept length $L_2(\alpha)$ of the polygon can be derived as

$$L_2(\alpha) = \frac{nacos(\frac{\pi}{n})}{4cos(\frac{\pi}{n}-\alpha)} \qquad (15)$$

It should be noted that the Eq. (15) is strictly valid within $[0, 2\pi/n]$, and it is a periodical function of $2\pi/n$ outside that region.

Figure 2 shows the d versus scan angle α for the polygons with even number of sides, the n values adopted are 4, 6, 8, 10, 12 and 20. It is clear that both the amplitudes and periods of d change as a function of n. The larger the n, the smaller the amplitude and the shorter the period. The amplitude is proportional to $cos(\pi/n)$. And it will approach zero when n goes to infinity, as is the case for circles.

Polar plots of d-α for rectangle, hexagon and ellipse were shown in Figure 3, 4 and 5. It is very interesting to note that d-α plots exhibit the same shapes as the real figures for regular polygons and circle. These plots also give a graphical description of the shapes studied and provide the best way to represent a shape. The polar d-α curves for rectangles and ellipses are, however, slightly different from the original shapes and they show as diamonds and quasi-ellipses, respectively.

2. Shape Index

Among these parameters mentioned above, the description of the grain or particle shape is the most difficult task encountered in the quantitative analysis. The prevailing approach in its characterization is to use arbitrarily defined shape factors or shape indices. Many models of shape factors have been proposed and were summarized by Underwood[4], DeHoff and Rhines[5] and Voort[6]. Since the shape factors are dimensionless, their definitions involve ratios of either the areas or the linear dimensions. For example, Hausner[7] has used the ratio of the square of the particle circumference L_p to $4\pi A$ to define a shape factor. The concept of shape factor is also used in engineering design to characterize the optimum shape of structures under different loading conditions[8,9].

It is evident that the d-α curve discussed above offer information not only about the average length but also about the shapes of the forms. This promoted us to define a shape index, SI, of a form as the area under its d-α curve. The definition of SI can be expressed as [1]

$$SI = \frac{1}{\alpha_p}\int_0^{\alpha_p} d\, d\alpha \qquad (16)$$

Where α_p is the period of the d-α curve. The shape index is then unity for circle and it will get smaller as the form becomes less circular. From above definition, the shape index of regular polygons with even number of sides is:

$$SI = \frac{cos\frac{\pi}{n}}{\frac{2\pi}{n}} ln\left(\frac{tan(\frac{\pi}{4}+\frac{\pi}{2n})}{tan(\frac{\pi}{4}-\frac{\pi}{2n})}\right) \qquad (17)$$

Equation (17) is plotted in Figure 6. It shows that SI gets greater as the polygon becomes more circular. The SI is practically equal to unity after $n > 20$.

It is important to note that the d-α curves of regular polygons with the odd number of sides do *not* fall between the curves for its neighbors with even number of sides. Instead, the d-α curve for equilateral triangle is exactly the same as that of the regular hexagon and d-α curve for the pentagon is identical to that of the decagon, and so on. This results from the fact that the tangent heights are the same for regular polygons with odd number sides and polygons with twice that number sides. However, the standard deviation of $L_2(\alpha)$ at any scan angle is much smaller for the latter than for the former, and this can be used as a differential factor. Another potential application of the d-α curve is that it can be used to study the plastic deformation of grains by comparing the shapes of the curve before and after plastic deformation. Since the analyzed area can be in the order of a few grains, local plastic deformation can be characterized.

3. Models for Elongated Polygons

In general the aspect ratios of grains or particles in question are not equal to unity as the grains are elongated in certain dimensions after plastic deformation. To model such microstructures formulae for a series of elongated polygons are derived in this work. These polygons are so designed that they have rectangle in the middle and their aspect ratios can be changed by varying the ratios of a/b of the rectangles. Each polygon can be viewed as a composition of several rectangles and triangles, and they can be classified as elongated pentagon, hexagon, heptagon and octagon. Their formulae for $L_2(\alpha)$ are listed in the Appendix. These models can be used to characterize the grains or particles with different aspect ratios. Figures 7, 8 and 9 show the d-α curves for these polygons with different b/a ratios. The length a in all the polygons is 1 to facilitate comparison. The intercept length d is a function of both n and scan angle α. The bumps in the curves reflect the periods of the original regular polygons. Another interesting point is that the d-α curves for these polygons become quite similar to one another when b/a is below 0.5.

4. Orientation Indices

If the linear intercept method is applied to a polycrystalline material with many grains, then it is necessary to define not only the overall SI_{all}, the integral of average d for all the grains along certain angle α, but also the shape index, SI, for each grain. If two grains are oriented at different angles with respect to the scan lines, their d-α curves will have a phase difference, i. e. one of the d-α curve will move along α axis for an angle relative to the other one. If the d in total d-α curve is the average over all grains in question, then the SI_{all} will reflect both the shapes and the orientations of all grains. If all the grains with their major axis oriented same way, then the SI_{all} will be the sole indication of the grain shapes. Otherwise, the SI_{all} will be greater than those of perfectly oriented grains and it will approach unity for statistically random oriented grain structure. Unless all the grains are perfectly oriented, one should then calculate the SI for each grain individually to evaluate the grain shapes and combine the SI_{all} to evaluate the texture of the major grain axes. Since d and orientation for all the grains in a polycrystal material are in general quite different, we define d_m as the average intercept length of m grains after rotating the grains and aligning them along their major axes. Thus, an average shape index SI_{avg} can be defined as:

$$SI_{avg} = \frac{1}{\pi}\int_0^{\pi} d_m \, d\alpha \qquad (18)$$

It is evident that SI_{avg} is the shape index without orientation effect while SI_{all} contains information on both shape and orientation. Since SI_{avg} represents the pure effect of shapes, one can thus

deconvolute the effects of shape and orientation effects. Consequently, an orientation index, Ω, is defined as:

$$\Omega = \frac{1\text{-}SI_{all}}{1\text{-}SI_{avg}} \qquad (19)$$

For a random oriented structure, SI_{all} will tend to be unity and Ω is equal to zero, and for a perfectly oriented structure the SI_{all} is equal to SI_{avg} and Ω is unity. Therefore, one can use Ω to quantitatively describe any degree of randomness using the scale from zero to unity.

To test the orientation index, grids of rectangles have been characterized using the linear intercept method. For a grid with all rectangles of same size, the d-α curve is exactly the same as the model predicts for a single rectangle, i.e. $SI_{all} = SI_{avg}$ and $\Omega = 1$. For the grid consisting of rectangles with different sizes but same aspect ratio, the size difference affects only the average intercept length, $L_2(\alpha)$. If d vs. α curve is plotted, the two grids will yield the same result. Thus the shape index defined here is independent of both the size and the size distribution of the grains.

A case of two rectangles perpendicular to each other was also studied. Fig. 10 is the d-α plots for each rectangle and for the overall structure. The shape index for each rectangle is 0.56 and for the whole structure, it is 0.74, a 32% change reflecting orientation difference.

Finally, we note that the orientation index defined here contains information about pure orientation of the major axes of the grains, and it does not carry any information about the crystallgraphic orientation of the grains.

EXPERIMENTAL

The grain structure of Al 7050-T7 plate alloy has been used to test the proposed models. The specimen preparation technique has been described in detail by Zhang et al[1]. The material has shown different grain structures along all three L, S and T directions. Figure 11 is the micrograph on L section in the middle of the plate. All parameters defined in this work have been estimated using a computer program developed specially for this purpose.

RESULTS AND DISCUSSION

Subgrains in Fig. 11 have been characterized individually to obtain the average intercept d and L_{II}, d-α plot and SI. Figure 12 is the plot of SI_{all} and SI_{avg} for the subgrains in Fig. 11. SI_{all}, which is the area under the d-α curve, is larger than SI_{avg} because of the effect of different grain orientations. The SI_{all} is 0.83, 18% increase due to the orientation effect. The degree of orientation can also be quantitatively evaluated based on SI_{all} and SI_{avg}. The orientation index, Ω, defined in Eq. (18) is 0.568.

In addition, the average grain aspect ratio was also obtain from the same plot, Fig. 12. The aspect ratio is the ratio of SI_{avg} at 0 and 90° and it is equal to 0.553 in this case.

The models of elongated polygons and ellipse derived above have been also used to characterize the grain structure in the alloy studied. The models of ellipse, elongated hexagon and octagon were used to fit the data by the least-square method. The shape index of the microstructure is 0.6998; it is thus between 0.7120 of an ellipse with $b/a = 0.5222$ and 0.6908 of an elongated hexagon with $b/a = 0.8352$ and 0.6947 of an elongated octagon with $b/a = 0.9072$. All three models give good fit to the experimental data and the quantitative description of the shape of the microstructure can be obtained by choosing the one with the best fit; in this particular case the octogon model is the best of the three models. Overall, the example demonstrated that the elongated polygon models are simple and

effective methods to quantitatively characterizing the shapes. Additionally, since the technique is independent of materials, it can be also used in other types of engineering materials or in any shape and orientation related problems.

CONCLUSIONS

1. The expressions for the average intercept lengths for simple geometrical shapes have been developed. These models can be used to study the effects of various shapes, both convex and concave, on the average intercept length and aspect ratio. Both x-y plot and polar plot of d-α have been used. The x-y plot provides quantitative measurement of the grain sizes while the polar plot gives graphic description of the shapes. The models can be applied to any homogeneous or heterogeneous microstructures.

2. A new shape index has been defined and it is based on the plot of the average intercept length vs. scan angle. The shape indices of simple forms, such as square, rectangle and ellipse, have been calculated. A formula for the shape index of regular polygons has also been derived. These shape indices can be used to quantitatively identify the shapes of grains and second phase dispersions.

3. An new orientation factor, Ω, has been introduced by utilizing the shape indices of each grain. This factor can be used to quantitatively describe the degree of randomness of structures.

4. Models for the elongated polygons have been proposed and applied to the characterization of the Al-7050 plate alloy. The analysis showed that the sizes and the aspect ratios of the polygons can be easily adjusted to suit different shapes of grains and particles.

Acknowledgment

The authors are grateful to Alcoa Laboratories for providing us with the material and to the Office of Naval Research for their support under Grant No. N00014-91-J-1299 of which Dr. A. K. Vasudevan is the program manager.

References

1. Jimin Zhang, Annetta J. Luevano and Marek A. Przystupa: "Quantitative Analysis of Heterogeneous Structures of Aluminum 7050 Alloy" Submitted to Scripta Metallurgia, (1991).
2. E. E. Underwood and S. B. Chakrabortty, Fractography and materials science, STP 733, 337; 1981, Pittsburg, PA, ASTM
3. S. I. Tomkeieff, "Linear Intercepts, Areas and Volumes", Nature, Vol. 155, pp24, January, (1945).
4. Underwood, E. E. Quantitative Stereology, Addison-Wesley Publishing Company, Reading, Massachusetts, pp196-197, (1970).
5. Robert. T. DeHoff and Fredrick N. Rhines: Quantitative Microscopy, McGraw-Hill Book Company, New York, NY 10036, USA (1968).
6. Vander Vroot, Metallography Principles and Practice, McGraw-Hill Book Company, New York, NY 10036, USA (1984).
7. Hausner, H. H.:"Characterization of the Powder Particle Shape," Planseeber. Pulvermetall., vol. 14, pp75-84, (1966).
8. Shanley, F. R. Weight-Strength Analysis of Aircraft Structures, 2nd edition, Dover, New York (1960).
9. Parkhouse, J. G. Structuring: a Process of Materials Dilution, in 3rd Int. Conf. on Space Structures, pp367 (edited by H. Nooshin). Elsevier London (1984).

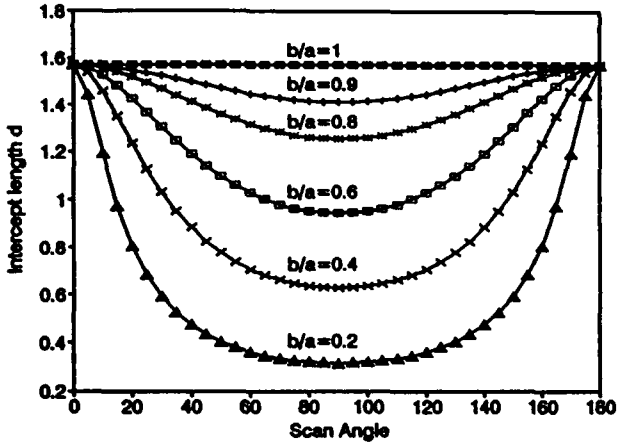

Fig. 1. Normalized intercept length, d, for ellipses with different b/a ratios.

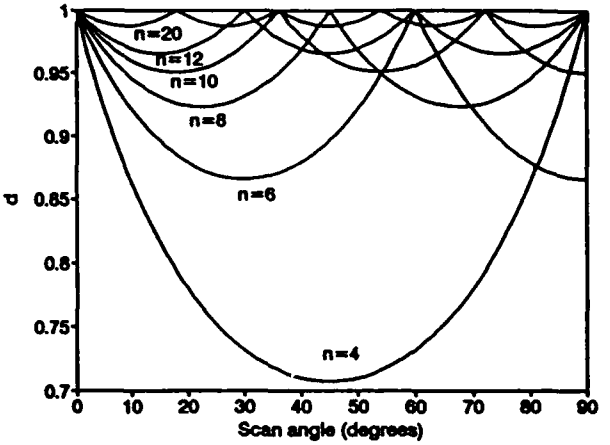

Fig. 2. Normalized intercept length, d, for regular polygons with n sides.

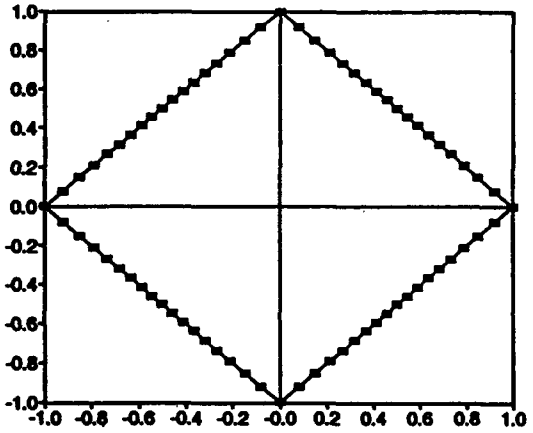

Fig. 3. Polar plot of d-α for a square.

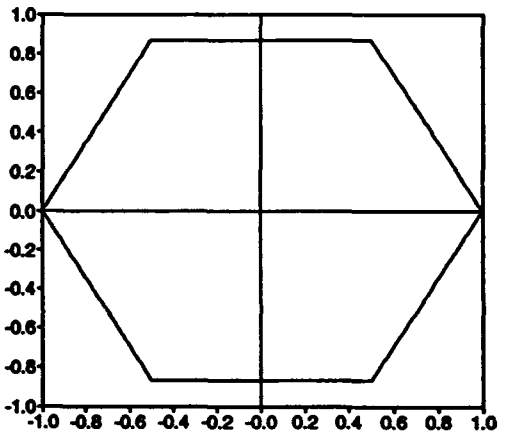

Fig. 4. Polar plot of d-α for a hexagon.

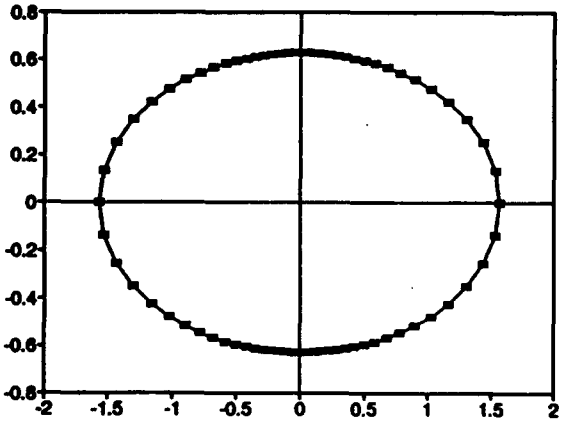

Fig. 5. Polar plot of d-α for an ellipse with b/a = 0.4.

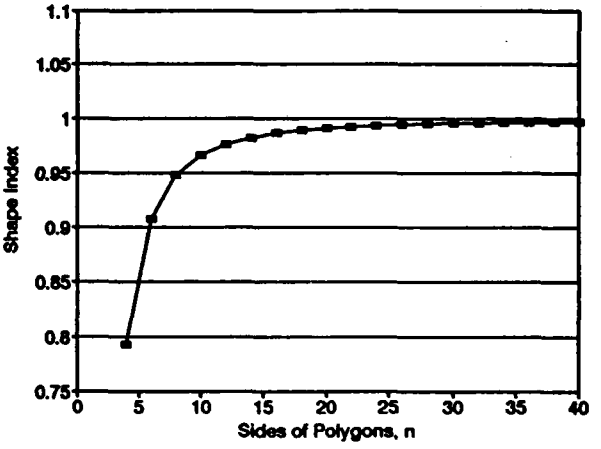

Fig. 6. Shape indices of regular polygons with n sides.

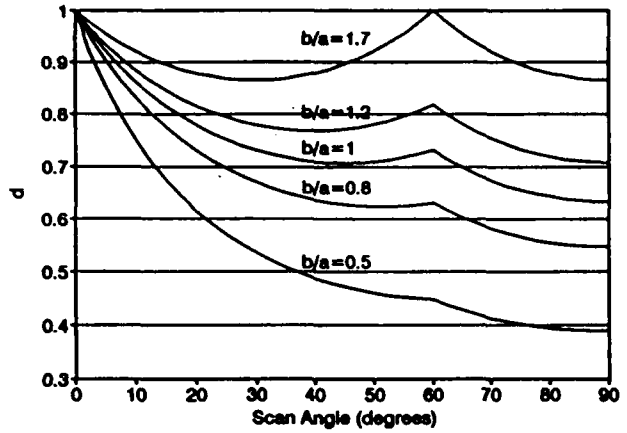

Fig. 7. Normalized intercept length, d, for elongated hexagons with different b/a ratios.

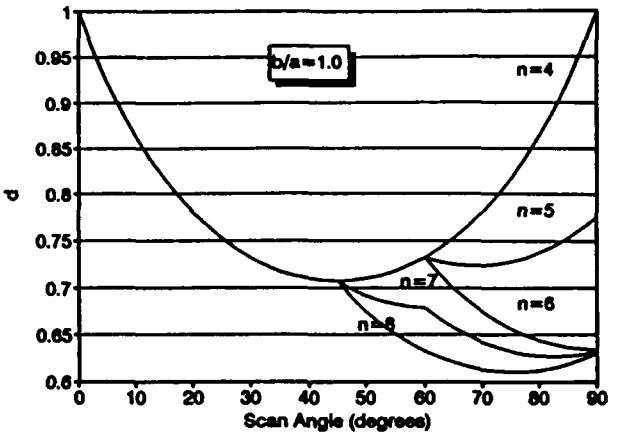

Fig. 8. Normalized intercept length, d, for elongated polygons with n sides.

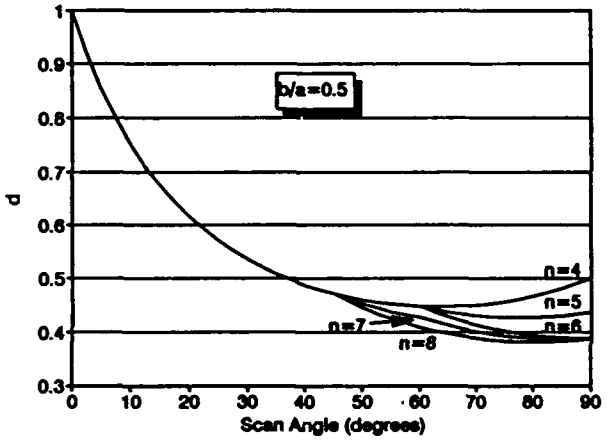

Fig. 9. Normalized intercept length, d, for elongated polygons with b/a=0.5.

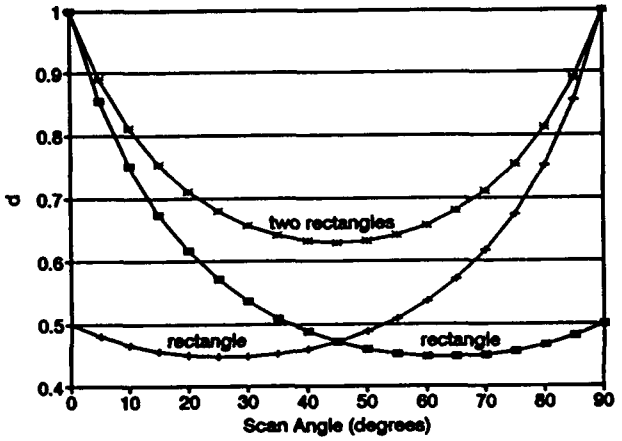

Fig. 10. Normalized intercept length, d, for a single rectangle and a structure with two rectangles perpendicular to each other.

Fig. 11. Subgrain structure of the 7050 Aluminum alloy.

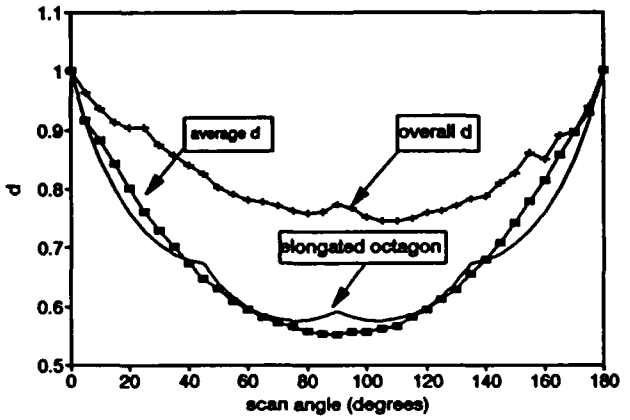

Fig. 12. Normalized intercept length, d, for the subgrain structure in Fig. 11.

APPENDIX

Rectangle:

$$L_2(\alpha) = \frac{a}{\cos\alpha + \frac{a}{b}\sin\alpha} \qquad \alpha[0,90] \qquad \text{(A1)}$$

Elongated pentagon:

$$L_2(\alpha) = \frac{a + \frac{b}{4\sqrt{3}}}{\cos\alpha + \frac{a}{b}\sin\alpha} \qquad \alpha[0,60] \qquad \text{(A2)}$$

$$L_2(\alpha) = \frac{a + \frac{b}{4\sqrt{3}}}{\cos\alpha + \frac{a}{b}\sin\alpha + \frac{\sin(\alpha-60)}{\sqrt{3}}} \qquad \alpha[60,90] \qquad \text{(A3)}$$

Elongated hexagon:

$$L_2(\alpha) = \frac{a + \frac{b}{2\sqrt{3}}}{\cos\alpha + \frac{a}{b}\sin\alpha} \qquad \alpha[0,60] \qquad \text{(A4)}$$

$$L_2(\alpha) = \frac{a + \frac{b}{2\sqrt{3}}}{\left(\frac{a}{b} + \frac{1}{\sqrt{3}}\right)\sin\alpha} \qquad \alpha[60,90] \qquad \text{(A5)}$$

Elongated heptagon:

$$L_2(\alpha) = \frac{a+\frac{b}{4\sqrt{3}}+\frac{b}{2(1+\sqrt{2})}}{\cos\alpha+\frac{a}{b}\sin\alpha} \qquad \alpha[0,45] \qquad \text{(A6)}$$

$$L_2(\alpha) = \frac{a+\frac{b}{4\sqrt{3}}+\frac{b}{2(1+\sqrt{2})}}{\frac{a}{b}\sin\alpha+\frac{\cos\alpha+\cos(\alpha-45)}{1+\sqrt{2}}} \qquad \alpha[45,60] \qquad \text{(A7)}$$

$$L_2(\alpha) = \frac{a+\frac{b}{4\sqrt{3}}+\frac{b}{2(1+\sqrt{2})}}{\frac{a}{b}\sin\alpha+\frac{\cos(\alpha-45)}{\sqrt{3}}+\frac{\sin(\alpha+45)}{1+\sqrt{2}}} \qquad \alpha[60,90] \qquad \text{(A8)}$$

Elongated octagon:

$$L_2(\alpha) = \frac{a+\frac{b}{1+\sqrt{2}}}{\cos\alpha+\frac{a}{b}\sin\alpha} \qquad \alpha[0,45] \qquad \text{(A9)}$$

$$L_2(\alpha) = \frac{a+\frac{b}{1+\sqrt{2}}}{\cos(\alpha-\alpha_1)\sqrt{\frac{1}{1+\sqrt{2}}+\frac{(1+\sqrt{2})^2a^2}{b^2}}} \qquad \alpha[45,90] \qquad \text{(A10)}$$

$$\alpha_1 = 90-\arctan\left(\frac{1}{\sqrt{2}+\frac{a}{b}(1+\sqrt{2})}\right) \qquad \text{(A11)}$$

APPENDIX 3

PRECIPITATE PHASE IDENTIFICATION AND GRAIN BOUNDARY PRECIPITATE CHARACTERIZATION OF THE ALUMINUM ALLOY 7050 IN THE T7 TEMPER, Annetta J. Luévano, Jimin Zhang and Marek A. Przystupa, Department of Materials Science and Engineering, University of California, Los Angeles, CA 90024

The microstructure of 7050 in the T7 temper has been characterized using a transmission electron microscope. Precipitate phases present in the grains and on the grain boundaries have been identified. The precipitate phases present inside the grains are η' and η. The ratio of grain boundaries containing precipitates to those without grain boundary precipitates has been calculated. Grain boundaries containing precipitates have also been characterized as to whether they are low angle or high angle. The specific variants of η common to the type of grain boundary have been characterized and the sizes of the precipitates have been measured. The density of precipitates in low angle grain boundaries is higher than that in high angle grain boundaries, while the precipitate sizes are larger in the latter. The widths of the precipitate free zones (PFZ's) present in the alloy have been measured and the volume fraction of precipitates in the PFZ's has been calculated. Any differences in the volume fraction of precipitates in the PFZ's associated with high and low angle grain boundaries will be discussed.

QUANTITATIVE EVALUATION OF GRAIN SIZES AND SHAPES OF ALUMINUM 7050 ALLOYS, Jimin Zhang, Annetta J. Luévano and Marek A. Przystupa,Department of Materials Science and Engineering,University of California, Los Angeles, CA 90024

Grain sizes and shapes of aluminum 7050 alloys in T7 condition have been investigated using image analysis techniques. The alloy was partially recrystallized and had great inhomogeneity through the thickness in both grain sizes and shapes: irregular recrystallized grains and pancake-shaped unrecrystallized grains were observed. An automated linear intercept method was used to measure the average grain sizes and the spherical harmonics were used to quantify the grain shape distributions. Since the alloy was partially recrystallized, both sizes and shapes of recrystallized and unrecrystallized grains and the degree of recrystallization were measured. The system used in the measurements can take images from different sources and is suitable for characterization of grains, second phase particles, pores and inhomogeneous materials such as composites. The advantage of this system is that it gives quantitative results and offers a multitude of information of how the material was processed and how it can be fully utilized. The results of all measurements, the measurement techniques and the correlation of the microstructure and the mechanical behavior of the alloy will be discussed in details.

THE EFFECT OF MICROSTRUCTURAL FLUCTUATIONS ON FATIGUE LIFE DISTRIBUTIONS IN ALUMINUM ALLOYS: Marek A. Przystupa, Jimin Zhang, Annetta J. Luévano, Department of Materials Science and Engineering, University of California, Los Angeles, CA 90024.

The distribution of fatigue lives, for identical loading conditions, depend on the local fluctuations in microstructure due to flaws, varying grain shapes, sizes and orientations, distributions of the second phase particle volume fractions, sizes and spacings, operating crack closure mechanisms, etc. The resulting effect from all above-mentioned microstructural inhomogeneities is a times to failure distribution curve, with different microstructural features affecting different parts of that curve. For instance; in aluminum alloys large porosities and non-deformable particles control general shape of the distribution curve and particularly its shape for the short failure times. On the other hand precipitates and grain structure control the shape of the tail of the distribution for long failure time. Furthermore, crack closure mechanisms can shift whole curve to longer or shorter times. This talk will address the question of the influence of all above factors on the shape of the fatigue life distribution curves using aluminum 7050 alloy as an example.

Work supported by the Office of Naval Research under Grant No. N00014-91-J-1299.